



Bisdithiocarbamate and Diamine Interlinked Gold Nanoparticle Networks: Characterization of Chemical Composition and Chemiresistive Properties

Tina Tauchnitz¹, Yelyena Daskal¹, Rosemarie Dittrich¹, Michael Günthel², Florian Mertens² and Yvonne Joseph^{1*}

¹Institute of Electronic and Sensor Materials, TU Bergakademie Freiberg, Freiberg, Germany, ²Institute of Physical Chemistry, TU Bergakademie Freiberg, Freiberg, Germany

OPEN ACCESS

Edited by:

Fabiana Arduini,
University of Rome Tor Vergata, Italy

Reviewed by:

Niravkumar J. Joshi,
Federal University of ABC, Brazil
Junseop Lee,
Gachon University, South Korea

*Correspondence:

Yvonne Joseph
Yvonne.Joseph@esm.tu-freiberg.de

Specialty section:

This article was submitted to
Micro- and Nano- Sensors,
a section of the journal
Frontiers in Sensors

Received: 29 March 2022

Accepted: 24 June 2022

Published: 25 August 2022

Citation:

Tauchnitz T, Daskal Y, Dittrich R,
Günthel M, Mertens F and Joseph Y
(2022) Bisdithiocarbamate and
Diamine Interlinked Gold Nanoparticle
Networks: Characterization of
Chemical Composition and
Chemiresistive Properties.
Front. Sens. 3:907443.
doi: 10.3389/fsens.2022.907443

Chemiresistive composites of gold (Au) nanoparticles interlinked with different types of organic molecules were prepared automatically by layer-by-layer self-assembly using a microfluidic cell. For the assembly process, dodecylamine-stabilized Au nanoparticles with an average size of 3.7 nm as well as alkyl dithiols, alkyl diamines, and alkyl bisdithiocarbamates with different alkyl chain length (C₆ and C₈) were used. X-ray photoelectron spectroscopy was applied on prepared nanoparticle composites to study the film composition and the degree of interlinkage. For the measurement of electrical and vapor-sensing properties, silicon dies equipped with gold interdigitated electrodes were used. All films show linear current-voltage characteristics and conductivities in the range of 10⁻² and 10⁻⁴ Ω⁻¹ cm⁻¹ at room temperature. The sensitivity of the film is investigated by dosing them with vapors of toluene, 1-propanol, 4-methyl-2-pentanone, and water in the concentration range from 100 to 5,000 ppm at 0% relative humidity. All composite films respond with an increase in their electrical resistance to the analytes. The sensors show a high signal-to-noise ratio which indicates a detection limit below 100 ppm for all test vapors. The response dynamics demonstrate a high reversibility and a fast sensing mechanism especially for dithiols and diamines with response and recovery times from 2 to 10 s. The dithiol sensors exhibit a high selectivity to toluene and 4-methyl-2-pentanone whereas the bisdithiocarbamate composites are suitable for the detection of water and 1-propanol. All materials are stable for (at least) several months.

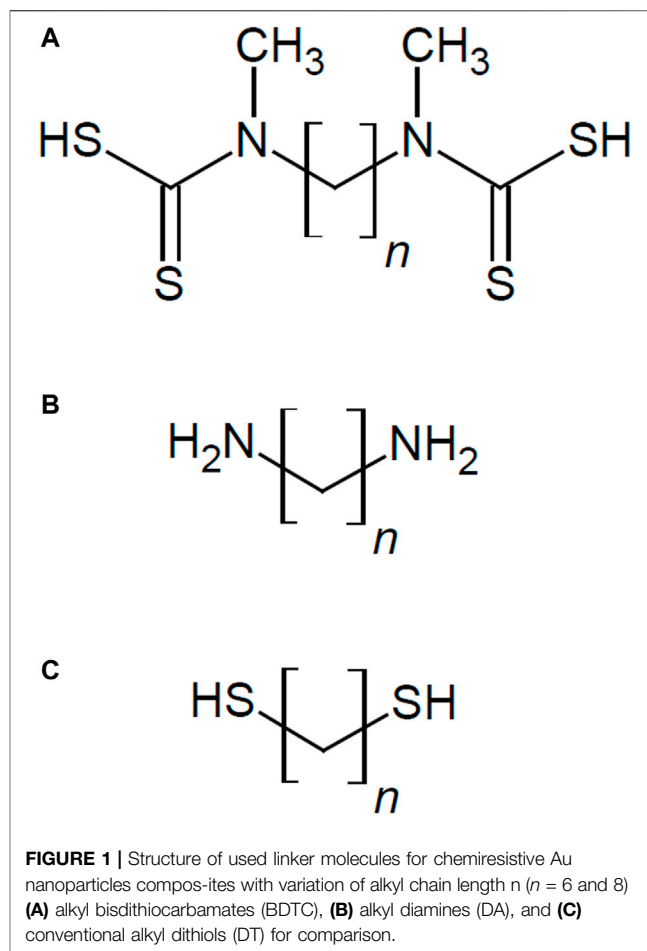
Keywords: chemiresistors, gold, nanoparticle, composites, XPS, dithiocarbamate, amine, volatile organic compounds

1 INTRODUCTION

Composite materials made of metallic nanoparticles have attracted considerable attention in materials research during the past few years (Shipway et al., 2000; Franke et al., 2006). Especially in the field of chemical sensors, nanoparticle composites are well-suited candidates for the detection of gases and vapors and offer a high-performance alternative to conventional metal

oxide or 2D materials gas sensors (Haick, 2007; Broza et al., 2018; Ehsani et al., 2021). Similar to other chemiresistors comprising of composite-materials, an advantage of nanoparticle-based sensors is seen in the possibility to operate at room temperatures that enables easy device integration and needs low power consumption (Hartwig et al., 2018; Ketelsen et al., 2018; Schlicke et al., 2020; Song et al., 2020). These composite can be prepared in very thin layers (<50 nm) resulting in very fast response and recovery times (t_{90} times usually in a few seconds) because of efficient diffusion of the analytes in the sensitive material. Furthermore, the selectivity can be tuned by careful selection of the inorganic and organic component, i.e. including of polar functional groups will change the selectivity towards hydrophilic compounds, while the introduction of hydrophobic groups will result in higher selectivity for nonpolar analytes. Different research groups have already reported on nanoparticle network sensors for gas and vapor detection especially to improve selectivity and sensitivity and to understand the sensing mechanism (Evans et al., 1999; Han et al., 2001; Krasteva et al., 2002; Zhang et al., 2002; Grate et al., 2003; Joseph et al., 2004; Wang et al., 2007; Potyrailo, 2017). In the development of metal nanoparticle composites, mainly Au and Pt particles were investigated (Vossmeier et al., 2002; Joseph et al., 2003; Krasteva et al., 2003; Joseph, 2004; Yang et al., 2006; Jiang et al., 2007). However recently, also semiconductor based nanoparticle composites were explored for chemical sensing (Samadi Khoshkhoo et al., 2018; Maiti et al., 2018; Samadi Khoshkhoo et al., 2019). Depending on the used particle material, different ligands or linker were studied (Potyrailo, 2017; Reichhelm et al., 2017). Au nanoparticle (AuNP) composites interlinked with bi- or polyfunctional dithiols (DT) are the most well-known sensing networks for gas and vapor detection (Vossmeier et al., 2002; Joseph et al., 2003), even if some dendritic polyfunctional amines or other sulfur based substances have been investigated (Yonezawa et al., 2001; Krasteva et al., 2002; Krasteva et al., 2003).

Despite the material itself, both the film thickness and film morphology of the nanoparticle networks have a dramatic influence on the sensor response. For the DT interlinked AuNPs, the film composition was investigated in detail indicating a quantitatively ligand-linker exchange during the assembly process (Joseph et al., 2003). Furthermore, the impact of film composition on the sensing properties as well as the sensing mechanism itself has been shown for DT linker in recent studies (Joseph et al., 2003; Joseph, 2004; Joseph et al., 2008; Toda et al., 2010). It has been shown that the sensing mechanism was dominated by swelling of the film material. In fact, solvent vapors are sorbed to the organic film components leading to film swelling while conventional gases are bound to vacant sites on the NP surface. In chemiresistors the swelling lead to either to an increase of resistance due to an increased interparticle tunnel distance while in freestanding membranes the resonance frequency changes (Schlicke et al., 2017; Squillacci et al., 2019). The swelling behavior of the composite strongly depends on the degree of interlinkage between NPs and linker molecules. The degree of interlinkage is consistent with the ability of the functionalized linker molecules to form more or less



chemical bonds with the NPs as well as with their stiffness. The lower the degree of interlinkage, the higher is the swelling ability of the film material. Another important fact that has to be taken into consideration to discuss the sensing mechanism is the filling process of solvent vapor species or gases into pores of the film material causing a decrease in the electrical resistance by a permittivity change in the organic matrix surrounding the nanoparticles. The formation of pores in the NP composite film is basically defined by the structure of the linker molecules and the degree of interlinkage. The pore filling process can be discussed on the basis of the composite densities. Summarizing, the total sensor response of NP composite films thicker than 10 nm represents a mixture of the chemical composition, the ability to swell, and a pore filling process.

Finally, to understand the electrical conductivity mechanism of conductive NP networks, the mathematical model of a thermally activated tunnel process has been discussed in several publications (Andres et al., 1996; Wuelfing et al., 2000; Joseph et al., 2003; Samadi Khoshkhoo et al., 2018). Two exponential terms are involved by the mathematical relation: The first exponential term takes into account the tunneling of charges between neighboring particles. The second exponential

expression includes the thermal activation of charge carriers. In the resulting network, the electrically conductive NPs are embedded in a dielectric matrix of organic linker molecules. The sensing ability of the films is a result of the manipulation of the interparticle tunnel distance by swelling or a change in the permittivity of the organic matrix if molecules are incorporated in the film structure.

The aim of the present research is the investigation of new organic linker molecules such as alkyl diamines (DA) and alkyl bisdithiocarbamates (BDTC) for vapor sensing chemiresistive AuNP composites. More specifically, 1,6-Hexanediamine (C6), 1,8-Octanediamine (C8), 1,6-Hexanebisdithiocarbamate (C6), and 1,8-Octanebisdithiocarbamate (C8) were used. In particular, we investigate the film composition, electrical properties and sensor characteristics to different hydrophobic and hydrophilic solvent vapor analytes. The sensing properties and mechanisms of the new interlinked and automatically assembled materials are highlighted and compared to conventional DT-based AuNP sensors with the same alkyl chain lengths. **Figure 1** shows the structure of the studied molecules.

2 EXPERIMENTAL SECTION

2.1 Materials and Film Preparation

Chemicals with reagent grade or higher purity were purchased from Sigma Aldrich, VWR and Acros Organics and used as received. 1,6-Hexanediamine, 1,8-Octanediamine, 1,6-Hexanebisdithiocarbamate and 1,8-Octanebisdithiocarbamate were used as organic linker molecules. Additionally, 1,6-Hexanedithiol, and 1,8-Octanedithiol were used for comparison. For the layer-by-layer self-assembly, the linker molecules were diluted in organic solvents. The DT linker were dissolved in toluene while the DA molecules were diluted in 2-propanol with concentrations of 5 mmol/L for both. In contrast, the BDTC had to be synthesized separately by *in-situ* because of their instability without solvent (Daskal et al., 2017). The BDTC linker solution had a concentration of 1 mmol/L while 2-propanol was used as the solvent in the catalysis procedure (see **Supporting Information** for more details on the synthesis procedure). Dodecylamine-stabilized AuNPs were prepared similarly to the wet-chemical method developed by Leff et al. (Leff et al., 1996) and had a core size of 3.7 ± 0.5 nm, as determined by transmission electron microscopy (TEM). The AuNPs were diluted in toluene with a concentration corresponding to an absorbance of 0.4, measured at the maximum of the plasmon absorption band ($\lambda_{\text{max}} = 512$ nm; 1 cm path length). Borosilicate cover slips with a defined thickness of 170 ± 5 μm and an edge length of 22 mm, obtained through Carl Roth GmbH, were used as substrates for x-ray photoelectron spectroscopy (XPS). For the electrical characterization, dies of silicon equipped with gold interdigitated electrodes characterized by a finger length of 5.2 mm, a height of 100 nm, and a spacing of the fingers of 50 μm (providing 52 finger pairs in total) were used as substrates. Furthermore, de-ionized water, acetone, hydrogen peroxide, and sulfuric acid were needed

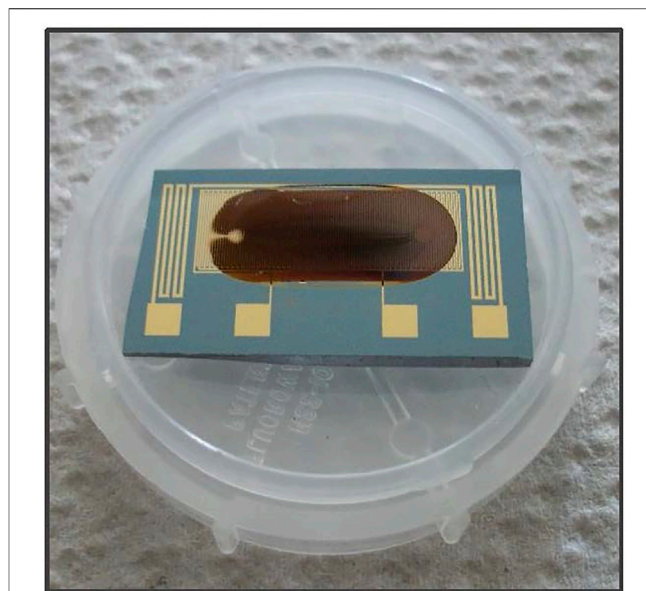


FIGURE 2 | Prepared composite film of 1,8-Octanediamine crosslinked AuNPs (DA AuC8) onto a silicon die equipped with gold interdigitated electrodes.

for substrate cleaning as well as 3-Mercaptopropyltriethoxysilane (MPTES) as silanization agent. Toluene, 4-methyl-2-pentanone, 1-propanol, and de-ionized water were employed as model solvent vapor analytes due to their comparable vapor pressures but different chemical structures.

For film preparation, the glass cover slips and silicon dies were cleaned for 15 min *via* ultrasonic in acetone, rinsed with de-ionized water, and then subjected to a Piranha ($\text{H}_2\text{SO}_4:\text{H}_2\text{O}_2$, 3:1, 90°C) solution for another 15 min. Afterwards they were thoroughly rinsed with de-ionized water and 2-propanol and blown dry with argon. The substrates were then immediately placed in a sealable glass apparatus for gas-phase silanization, with the silane previously heated to 120°C in an oil-bath, and the silane vapor, was guided over the substrates. After silanization, the substrates were placed into a home-made cross flow cell for coating with the sensing material. The automated layer-by-layer self-assembly process was described previously, including the discussion of the growth behavior of the composite films (Daskal et al., 2017). During the layer-by-layer self-assembly process, AuNP solution, organic solvent, linker solution, and organic solvent were alternately passed through the flow cell with a pump rate of 100 $\mu\text{L}/\text{min}$. The typical flow time sequence consists of 5 min/4 min/5 min/4 min with respect to the above mentioned order of solutions. In general, each organically interlinked AuNP composite film was prepared by 18 assembly cycles. In case of the assembly of DA and BDTC, the organic solvent had to be changed automatically from toluene to 2-propanol twice within an assembly cycle due to their solubility properties. After preparation, the films were purged with toluene for 10 min inside of the flow cell and dried by vacuum extraction. Finally, the prepared samples were stored in a desiccator under Ar atmosphere until they were used for

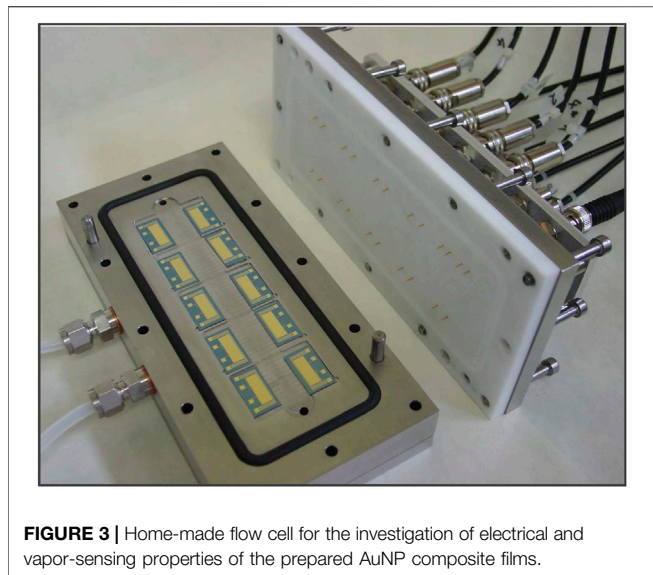


FIGURE 3 | Home-made flow cell for the investigation of electrical and vapor-sensing properties of the prepared AuNP composite films.

measurements. **Figure 2** shows an example of a prepared DA AuC8 composite film onto a silicon die. Layer thicknesses were measured with an Alpha-Step 500 profiler (KLA Tencor).

2.2 Characterization Methods

The chemical composition of the samples was examined using a SPECS XPS system with a PHOIBOS 150 MCD-9 hemispherical analyzer and a monochromatic Al K_{α} X-ray source operated at 1,486.6 eV and 200 W. All XPS measurements were performed with an absolute pressure lower than $5 \cdot 10^{-10}$ mbar. The spectra were recorded with a pass energy of 10 eV and a step size of 0.05 eV. The binding energy (BE) scale was calibrated to the Au $4f_{7/2}$ peak at 84 eV. For all spectra, a linear background was subtracted before the peak fitting with Voigt profiles (30% Lorentz, 70% Gauss) was performed. The spin-orbit splitting for S 2p was set to 1.18 eV. The respective intensity ratio was kept at 4:3 (Au $4f_{7/2}$:Au $4f_{5/2}$) and 2:1 (S $2p_{3/2}$:S $2p_{1/2}$). The atomic ratios of the film materials were determined from the integral intensities of the signals which were corrected by Scofield sensitivity factors (C 1s = 1.00, S 2p = 1.68, Au 4f = 17.10, N 1s = 1.80). The effect of electric charge offset could be fully eliminated by a special specimen holder avoiding an operation with a flood gun.

For investigation of electrical properties and chemical sensitivity of the AuNP composites, silicon dies with the sensor film on top can be mounted and measured simultaneously in a home-made flow cell. The specific test cell is shown in **Figure 3**. Current-voltage (I-V) measurements were carried out at room temperature ($\sim 22^{\circ}\text{C}$) using a home-built setup comprising of a Keithley 2612 SourceMeter and a Keithley 7001 SwitchSystem. In all I-V measurements, a voltage range of -1 V to $+1$ V and a current limiting of 0.1 A were employed. In order to study the chemical sensitivity, a constant direct current was applied to the sensors and the change of voltage across the electrodes was measured during switching between pure carrier gas and the analytes. The sensors were operated at a bias voltage of 0.1 V and a current limiting of 0.1 A. The sensor responses

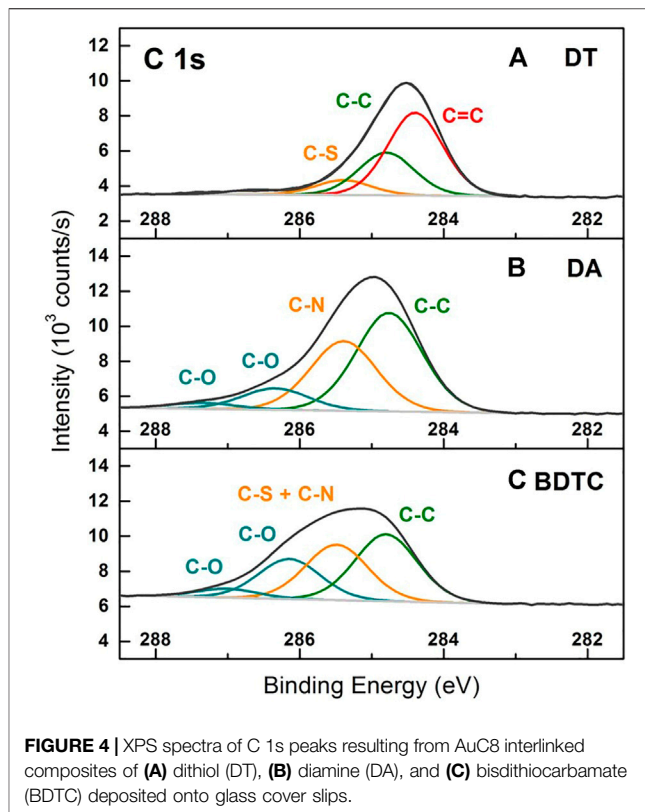


FIGURE 4 | XPS spectra of C 1s peaks resulting from AuC8 interlinked composites of (A) dithiol (DT), (B) diamine (DA), and (C) bisdithiocarbamate (BDTC) deposited onto glass cover slips.

were recorded as the relative change of their electrical resistance ($\Delta R/R_{\text{ini}}$). The baseline drift was corrected by subtracting a linear baseline (slope: 0.03 – 0.05% min^{-1} depending on the linker type). Test vapors (toluene, 4-methyl-2-pentanone, 1-propanol, de-ionized water) were provided using a commercial gas calibration system (Kalibriersystem MK15/MK5 or MK15-DDS-RL/MK5, Umwelttechnik MCZ GmbH, Ober-Mörlen, Germany) and applied within a concentration range of 100–5,000 ppm. The gas concentrations have been calibrated regularly with a photoacoustic detector. Argon was used as carrier gas for the test vapors, which was taken from a gas cylinder. The continuous gas flow was adjusted to 400 ml/min to enable a fast exchange of the vapors in the measurement cell. In all experiments the temperature inside the test cell was kept at room temperature ($\sim 22^{\circ}\text{C}$). The films were purged with argon for 6 h prior to all measurements in order to enhance desorption of humidity, contaminants, and solvents.

3 RESULTS AND DISCUSSION

3.1 Film Composition

Overview XPS spectra of the AuNP composite films show signals from Au, C, S, and N. Additionally, low Si and O signals were detected resulting clearly from silicon dioxide used as substrates for non-electrical measurements. **Figures 4–6** show the corresponding regions and components of the C 1s, S 2p, and N 1s peaks of AuC8 films comparing the different linker types.

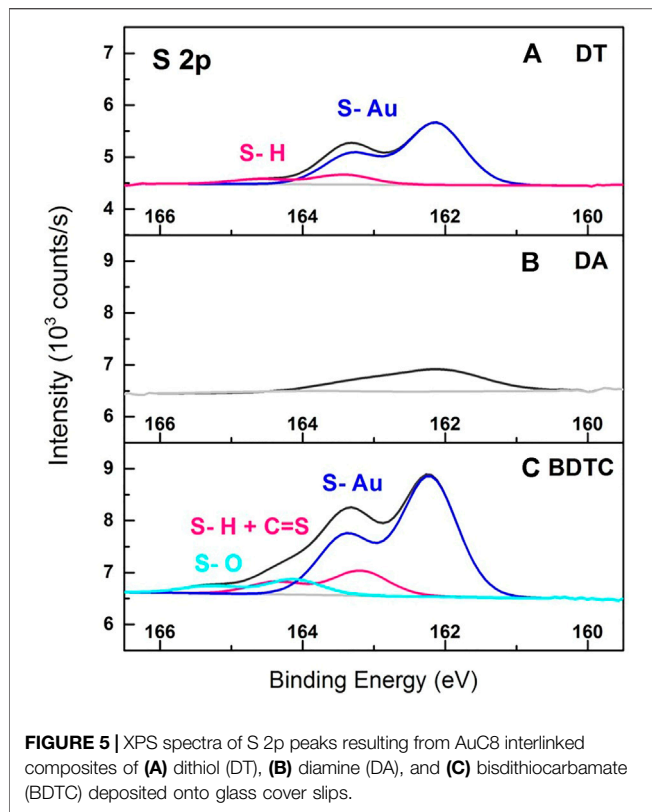


FIGURE 5 | XPS spectra of S 2p peaks resulting from AuC8 interlinked composites of (A) dithiol (DT), (B) diamine (DA), and (C) bisdithiocarbamate (BDTC) deposited onto glass cover slips.

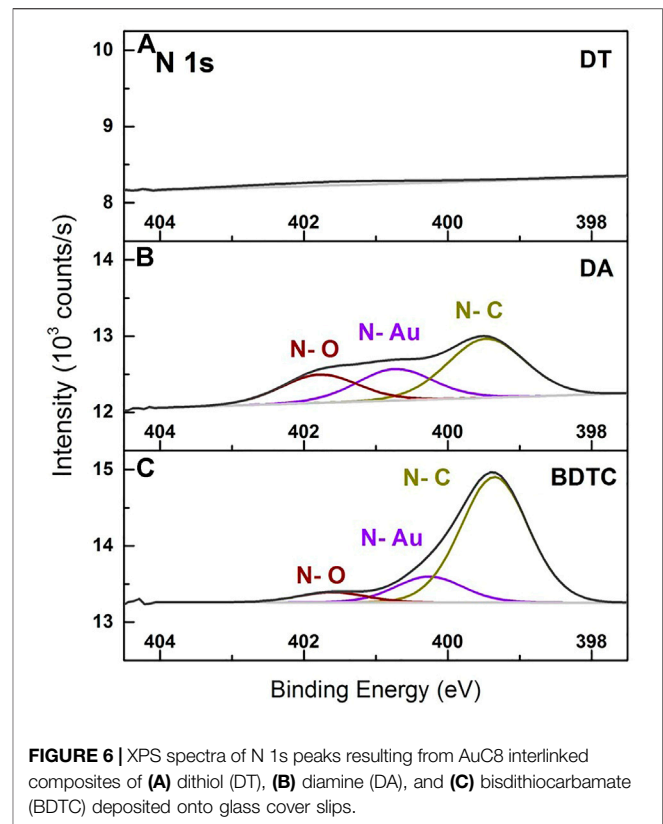


FIGURE 6 | XPS spectra of N 1s peaks resulting from AuC8 interlinked composites of (A) dithiol (DT), (B) diamine (DA), and (C) bisdithiocarbamate (BDTC) deposited onto glass cover slips.

The other films gave very similar spectra with respect to their peak shapes and positions.

3.1.1 Qualitative XPS

The C 1s peaks in **Figure 4** were fitted with four G-Lorentz functions. The DT interlinked composites (**Figure 4A**) reveal an aromatic carbon compound at 284.4 eV as the major component that results most probably from residual solvent (toluene). The component at 284.8 eV is related to aliphatic carbon that is in good agreement with reported data for AuC12 and AuC16 DT (Joseph et al., 2003; Joseph et al., 2009). According to the literature, carbon bound to sulfur was found at 285.4 eV (Joseph et al., 2003). A minor carbon component (smaller than 4% of the overall C 1s signal) was observed at higher BE that might be the result of an oxidized carbon species. In addition, no nitrogen signal was detected due to the full exchange of dodecylamine ligand to thiol groups. In comparison, in DA and BDTC based AuNP composites (**Figures 4B,C**), no aromatic carbon compound was found that might be explained by solvent exchange from toluene to 2-propanol within an assembly cycle. More specifically, the inclusion of solvents in the composite films may result primarily from the solvent in which the linker molecules were diluted and its solvent properties. Instead of aromatic carbon, the AuNP composites with interlinked DA and BDTC show aliphatic carbon as the major component at 284.8 eV. The DA films were characterized by carbon bound to nitrogen at 285.4 eV. Due to nearly the same BE of carbon bound to sulfur, the signals cannot be distinguished between C-N and C-S in the BDTC composites. Hence, the

component peak at 285.5 eV was assigned to a summation of C-N and C-S signal. Interestingly, DA as well as BDTC interlinked films include two species of oxidized carbon at BE larger than 286.0 eV. Their higher oxygen content could also be explained by the 2-propanol consisting of a functional hydroxy group that was used during the linker assembly step.

Figure 5 shows the S 2p signals of AuNP composites crosslinked with DT, DA, and BDTC. In general, the S 2p signal of the DT film shown in **Figure 5A** was fitted with two sum functions, where one function was assigned to sulfur bound to gold (S-Au) at 162.1 eV and the second function was correlated to the thiol component (S-H) at 163.4 eV according to the literature (Joseph et al., 2003). Surprisingly, the DA films indicated in **Figure 5B** also reveal a very small, but negligible sulfur component that mainly corresponds to S-Au at 162.0 eV and may originate from MPTEs employed as silanization agent (**Figure 5C**). In contrast to the DT composites, the BDTC films (**Figure 5C**) were fitted with three species. One S-Au component was detected at 162.2 eV as the major signal. Consequently, both sulfur species of one functional group of the BDTC molecule were bound symmetrically to the AuNP surface. This was already shown by studies of Morf and co-workers on self-assembled monolayers of dithiocarbamates (Morf et al., 2006). Another peak was related to unbound S-H components at 163.1 eV. Interestingly, the BE of unbound S-H of the BDTC composite is 0.3 eV smaller than that of the DT film at 163.4 eV indicating differences in the electronic structure of the functional group of the linker (Morf et al., 2006). Therefore, it is suggested that the

TABLE 1 | Atomic ratios (in at%) of elements/species and ratios between elements/species in the film material as determined by XPS. 1) Stoichiometry of linker (a) from measured data and (b) theoretical stoichiometry, 2) degree of interlinkage and 3) particle/linker ratio.

Linker Type	Au4f		C1s			S2p		N1s			(1)	(2)	(3)
DT	84.0	C=C 284.4	C-C 284.8	C-S 285.4	S-Au 162.1	S-H 163.4	—	—	—	—	C/S (a) (b)	S-H/S	Au/S-Au
AuC ₆	52	21	11	3	11	2					2.8 3.0	0.1	4.7
AuC ₈	45	25	13	5	10	2					3.6 4.0	0.1	4.5
DA		C-C	C-N	C-O	S-Au	—	—	N-C	N-Au	N-O	C/N (a) (b)	N-C/N-Au	Au/N-Au
BE (eV)	84.0	284.8	285.4	286.3/ 287.3	162.0			399.5	400.7	401.8			
AuC ₆	40	29	15	7	4			2	2	1	10.2 3.0	1.4	26.1
AuC ₈	41	27	18	7	3			2	1	1	10.5 4.0	1.9	33.2
BDTC		C-C	C-S + C-N	C-O	S-Au	S-H + C=S	S-O	N-C	N-Au	N-O	C/S (a) (b)	S-H/S	Au/S-Au
BE (eV)	84.0	284.8	285.5	286.1/ 287.0	162.2	163.1	164.0	399.4	400.3	401.6			
AuC ₆	33	18	14	11	13	3	2	4	1	1	2.3 2.5	0.2	2.5
AuC ₈	34	17	14	11	13	3	2	4	1	1	2.3 3.5	0.2	2.6

electronic structure of the functional C=S group as well as the molecular backbone of the BDTC linker is also included in this peak signal resulting in the slightly shifted peak position to lower BE. Finally, a small peak that can be attributed to an oxidized sulfur compound (S-O) was found at higher BE of 164.0 eV.

The N 1s peaks of DT, DA, and BDTC interlinked AuNPs are shown in **Figure 6**. As can be seen in **Figure 6A**, the DT composite film does not consist of any nitrogen compound highlighting the complete exchange of dodecylamine ligands during the automated assembly process. The N 1s signals of DA and BDTC (**Figures 6B,C**) were fitted with three G-Lorentz functions. The major component of the DA composite is the nitrogen bound to carbon at 399.5 eV, which represents the chemical bond of the functional group to the backbone of the linker molecule as well as of the dodecylamine ligands. The second major component is assigned to nitrogen bound to gold (N-Au) at 400.7 eV, which indicates that chemical bonds between the amine groups and the NP surface are formed. Due to the same functional amine groups of linker and stabilizing dodecylamine ligand, it cannot be distinguished by XPS whether a linker or a ligand is bound to the Au surface. Only a small contribution of the N 1s signal is related to an oxidized or charged species of nitrogen (N-O) at 401.8 eV. In comparison to the DA linker, compounds with nearly the same peak positions were observed qualitatively for the BDTC composite film. The N-C component also stems either from the linker or the dodecylamine ligand. But in contrast to the DA, the N-Au peak clearly indicates that residual dodecylamine ligands are still present on the surface of the NPs and have not been replaced by BDTC during the assembly process, or by the binding of the secondary amine that has not reacted in the *in-situ* linker formation process with CS₂. The decreased N-Au compound ($\Delta = \sim 10$ at%) and the increased N-C component ($\Delta = \sim 28$ at%) compared to the N 1s DA peak signal suggest a more effective assembly behavior of BDTC due to the strong N-C-S-Au bonding compared to the DA linker. An oxidized or charged nitrogen species was found in the BDTC film, too.

3.1.2 Quantitative XPS

The atomic ratios of elements detected in the film material (Au, C, S, N) were calculated from the integrals of the XPS signals, where the oxidized species as well as the impact of the substrate material were neglected. **Table 1** summarizes the atomic ratios of the elements in the film material.

The quantitative analysis of the DT films shows an increase of the carbon content on the surface with increasing chain length that is accompanied by a decrease of the gold content as expected. For the DA films, the atomic ratios of Au, C, and N remain constant as a function of chain length. The DA films exhibit a higher carbon content in comparison to the DT films presumably due to the inadequate exchange of dodecylamine ligands with the DA linker as discussed above. The BDTC films offer consistent atomic ratios of Au, C, S, and N as well. The total C 1s carbon ratio of the BDTC composites is comparable to those of the DT films. The BDTC composites contain twice as much sulfur as DT films due to the binding of two sulfur atoms in one functional molecule group (see XPS signal in **Figure 5**). Furthermore, the N-C content of the BDTC has doubled compared to the one of the DA composite whereas the N-Au component remains constant indicating that much more BDTC linker is bound to AuNP surface (see XPS signal in **Figure 6**). To study the impact of the molecule chain length on the atomic ratios, the number of -CH₂ units must be varied more significantly. For the DT linker, the dependency of the measured atomic ratios on the alkyl chain lengths is already presented in the literature (Joseph et al., 2003).

For clarification of the assembly and interlinkage of AuNP composites, ratios between different elements or species were calculated and summarized in **Table 1**. The ratios of carbon to sulfur are in reasonable agreement with the theoretical stoichiometry of the linker molecules, validating the sensitivity factors used for carbon and sulfur (theoretical C/S stoichiometry: DT: C₆ 3.0; C₈ 4.0; BDTC: C₆ 2.5; C₈ 3.0). In consideration of the carbon to nitrogen ratios of the DA composites, the calculated ratios of C₆ (10.2) and C₈ (10.5) are not in good agreement with

the theoretical C/N stoichiometry of 3.0 and 4.0. This suggests again a higher dodecylamine content in the composite films due to an insufficient exchange behavior of the DA molecules.

To evaluate the ability of the functionalized linker molecules to form chemical bonds with the Au surface, the degree of interlinkage is studied. The S-H/S ratio listed in **Table 1** represents the relative amount of thiol groups which are not bound to the AuNPs. The DT films include ~10 at% of free thiol groups. This means that ~80 at% of the DT linker molecules are attached on both ends to the AuNPs resulting in a very high degree of interlinkage. The BDTC composites contain ~20 at% of unbound S-H groups implying that ~60 at% of the BDTC linker are doubly bound to the AuNPs, which still corresponds to a high degree of interlinkage. Regarding the DA composites, the N-C/N-Au ratio describes the amount of linker or ligand bound to AuNPs. For instance, for the DA AuC8 composites, the N-C/N-Au ratio is nearly 2:1, which suggests that, next to the dodecylamine ligand, the DA linker molecule is also bound most probably on one end to the AuNP that leads to a small degree of interlinkage due to the insufficient assembly efficiency of DA. Consequently, the exchange of ligands against linkers is based on a statistical procedure, in which functional amine groups with homogeneous binding strength to AuNPs have to be exchanged, which results in an uncontrollable film assembly.

The Au/S-Au and the Au/N-Au ratio describe the relative particle/linker ratio which is roughly the same if one type of linker molecule is considered, and thus, independent on the alkyl chain length. Due to the binding of both sulfur atoms of one functional BDTC group, the particle/linker ratio is halved for BDTC composites (~2.5) compared to the DT films (~4.6) possibly reflecting the larger head groups of the BDTC. The poor film assembly of DA composites results in an extraordinarily high particle/linker ratio of larger than 26 confirming the low degree of DA interlinkage.

3.2 Film Porosity and Electrical Conductivities

The film thicknesses d_{film} investigated by profilometer measurements are given in **Table 2**. As can be seen, the film thickness varies between 20 and 92 nm, although all films were deposited with the same number of assembly cycles implying a change in film density in dependence of the different linker types and alkyl chain length. This is important as lower density may account for a higher amount of fillable pores. According to the literature (Daskal et al., 2017), the AuC6 and AuC8 DT films exhibit the highest film density of 11.0 and 9.7 g/cm³ compared to DA (AuC6: 7.8 g/cm³, AuC8: 6.0 g/cm³) and BDTC composites (AuC6: 4.6 g/cm³, AuC8: 2.8 g/cm³). Therefore, the DT composites form less porous very compact films due to the linear molecule structure and the high degree of interlinkage. Interestingly, the DA composites also offer intermediate densities. Because of the long-chained (not exchanged) dodecylamine ligands and the small degree of interlinkage of the DA composites, the films may offer a higher fraction of pores that are enclosed in the composite compared to the DT films. Highly interlinked, but highly porous BDTC AuNP films with

low densities were formed presumably due to the steric hindrance caused by the larger and branched structure of the head group of the relatively long BDTC molecule. The length of the different linker molecules are listed in **Table 2**.

As presented in **Figure 7** and **Table 2**, all composite films provide linear current-voltage characteristics and electrical conductivities in the range of 1.2×10^{-2} to $2.7 \times 10^{-4} \Omega^{-1} \text{cm}^{-1}$ at room temperature. Composites with shorter length of the organic molecules ($n = 6$) have higher conductivities, i.e. steeper I-V curves than composites with longer length of the organic molecules ($n = 8$). Composites of DT and DA with the same alkyl chain length exhibit comparable electrical conductivities in the order of 10^{-2} and $10^{-3} \Omega^{-1} \text{cm}^{-1}$. AuNP films crosslinked with BDTC are characterized by lower conductivities (AuC6: $10^{-3} \Omega^{-1} \text{cm}^{-1}$; AuC8: $10^{-4} \Omega^{-1} \text{cm}^{-1}$) because of the higher molecular lengths resulting from the considerable longer functional groups. In general, the room temperature conductivities are comparable to the literature (Joseph et al., 2003; Joseph et al., 2007; Joseph et al., 2008). The linear current voltage curves (cf. Joseph et al., 2008), the very low substrate XPS signals as well as the relatively high thicknesses imply the existence of a closed and homogenous film.

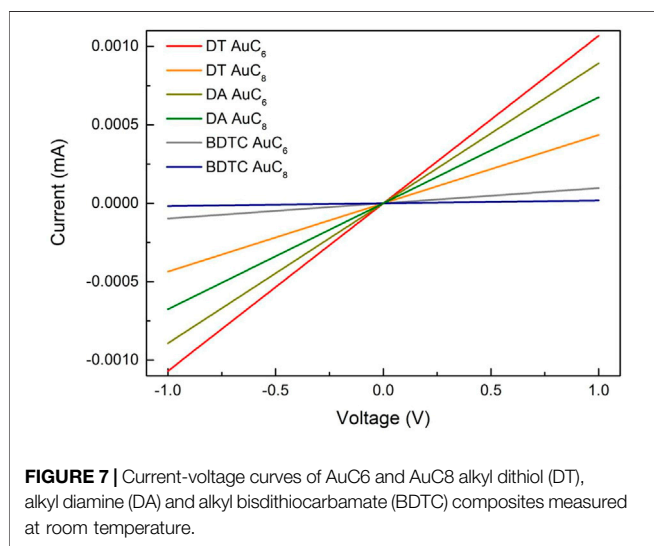
For visualization, a graphical binding model for each type of linker molecule was developed by extracting the chemical and structural information of all AuNP films. **Figure 8A** illustrates dodecylamine protected nanoparticles where no chemical interlinkage occur. However, van-der-Waals interactions are present between the hydrophobic chains. **Figure 8B** shows the dithiol interlinked AuNP networks. Here, most of the dithiols chemically interlink effectively the nanoparticles and a relative dense film can be observed, even if some free thiols can be observed. **Figure 8C** gives the structure of diamine-interlinked films. Here, a weaker ligand-linker exchange occur, due to the similar nature (and binding strength) of the functional groups and a lot of dodecylamine ligands are still present in the assembly. In **Figure 8D** the bisdithiocarbamate-interlinked assemblies are visualized. The bulkier functional groups are bidentately bound, blocking more binding sites compared to the dithiols and thus prevent a denser packing of the alkyl chains due to sterically hindrances and a smaller particle-to-linker ratio can be observed. Furthermore, not all ligands have been exchanged. As a result, the film is more porous.

3.3 Vapor-Sensing Properties

Figure 9 shows the sensor responses of the composite films while dosing them with toluene, 4-methyl-2-pentanone, 1-propanol, and water using an analyte concentration of 5,000 ppm. All composite sensitive films show only a slight baseline drift of approximately 0.03 (DT) to 0.05% min⁻¹ (BDTC) and reveal an increase in their relative electrical resistance, which indicates the induced swelling of the film materials as the sensor mechanism. The composite swelling appears due to the adsorption of solvent vapor analytes to the organic film components, which leads to an increased interparticle distance. The sensing mechanism for DT films is already described in the literature (Joseph et al., 2003; Joseph et al., 2008) wherein three possible sorption sites are reported: Hydrophobic and hydrophilic sorption sites are

TABLE 2 | Film thickness d_{film} , resistance R , room temperature conductivities σ_{RT} of organically interlinked AuNP composites as well as calculated lengths L_{linker} of linker molecules using a molecular force field approach (Xue et al., 2014).

Linker Type	Chain Length	d_{film} (nm)	R (k Ω)	σ_{RT} ($\Omega^{-1}\text{cm}^{-1}$)	L_{linker} (\AA)
DT	AuC ₆	23.8	0.3	3.8×10^{-2}	9.4
	AuC ₈	20.3	2.3	5.7×10^{-3}	11.9
DA	AuC ₆	24.3	1.1	1.2×10^{-2}	8.8
	AuC ₈	24.0	1.5	8.1×10^{-3}	11.2
BDTC	AuC ₆	87.0	10.3	1.1×10^{-3}	13.5
	AuC ₈	92.0	56.6	2.7×10^{-4}	15.5

**FIGURE 7** | Current-voltage curves of AuC₆ and AuC₈ alkyl dithiol (DT), alkyl diamine (DA) and alkyl bisdithiocarbamate (BDTC) composites measured at room temperature.

provided by the organic matrix; other sorption sites are derived from the organic-free parts of the metal NP surface. Due to the increased relative electrical resistance, the swelling-induced sensor mechanism can be applied for DA and BDTC composites as well.

As described earlier for film thicker than 10 nm (above the percolation threshold), the total sensor response represents a mixture of the amount of sorbed analytes (depending on the chemical compositions of the films and analyte molecules), the swellability, and the pore filling process of NP composites. The chemical composition of the AuNP films provides preferential sorption sites, and that in turn, determines the type of detectable analytes (i.e. hydrophilic, hydrophobic). Therefore, the chemical composition of AuNP networks affects the sensitivity and selectivity as the sensor properties. The swelling behavior of the composite strongly depends on the degree of interlinkage between NPs and linker molecules. The pore filling process is determined by the film density that is defined basically by the structure of the linker molecules. In any case, the pore filling process changes the chemical composition of the sensor films in the surrounding organic matrix and thus participates in the sensing mechanism.

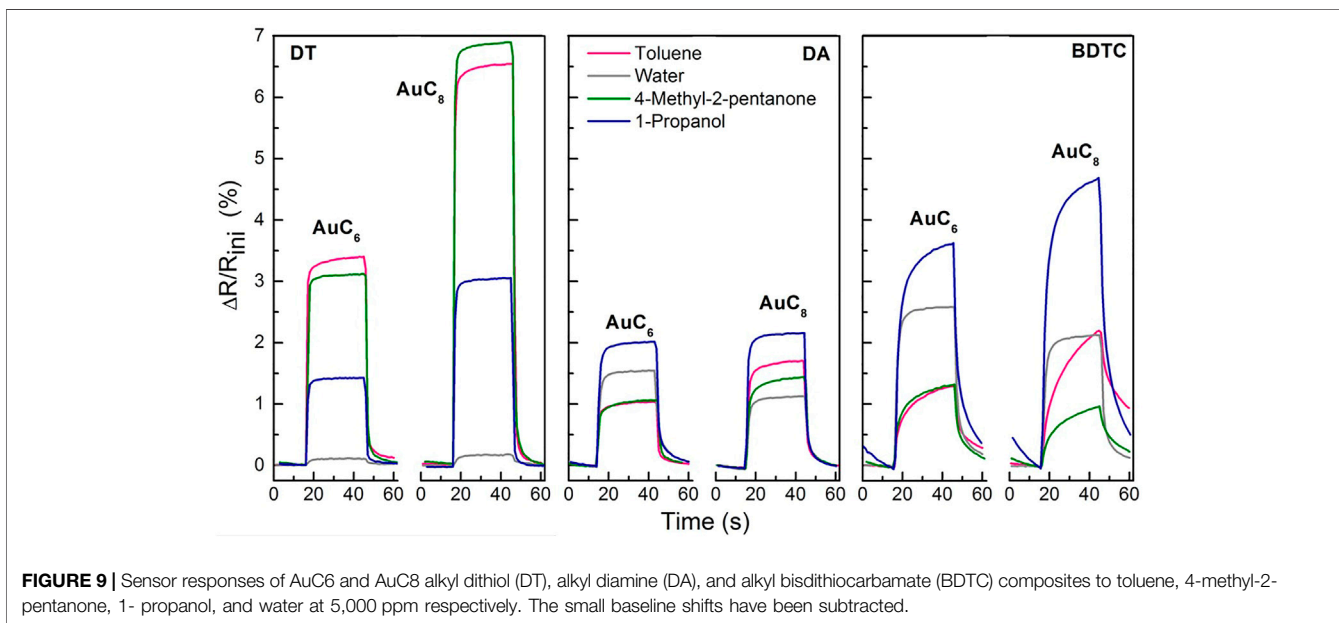
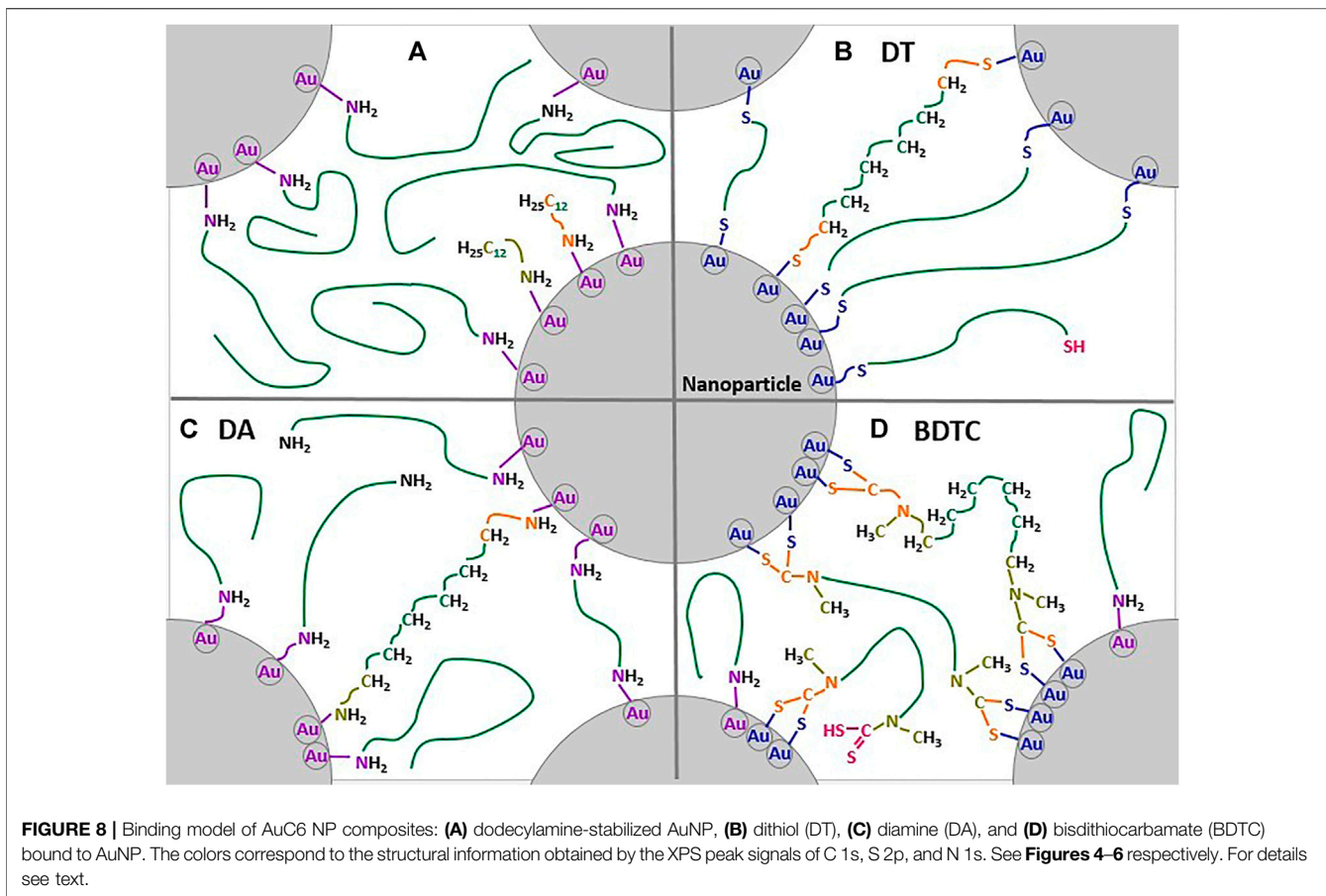
3.3.1 Sensitivity and Selectivity

As can be seen in **Figure 9**, the DT composites offer the highest sensitivities to the hydrophobic analytes toluene and 4-methyl-2-

pentanone due to the adsorption to the hydrophobic alkylene chains of the DT linker. The hydrophobic ends of 1-propanol are assumed to weakly adsorb to the alkyl chain, which results in a smaller sensor response. Because of the very small sensor response, it is quite obvious that water molecules only adsorb on the hydrophilic functional groups consisting of sulfur atoms. The sensitivity of the DT sensors correlates clearly with the alkyl chain length because of a better ability to swell as shown before (Joseph et al., 2003; Krasteva et al., 2003). The high swellability of DT sensors as well as the insignificant porosity due to the high density of DT films lead to the highest sensor response for hydrophobic analytes compared to DA and BDTC sensors. Summarizing, DT sensors are very selective to solvent vapors with hydrophobic molecule structure.

The DA composites reveal the highest sensitivities to the hydrophilic analyte 1-propanol (2.0% for AuC₆; 2.2% for AuC₈). The sensors offer increased swellability because of the low degree of interlinkage between DA linker and AuNPs. The DA composites do not possess a high porosity as indicated by the measured moderately high film density. Primarily, the non-polar end of the 1-propanol molecule is able to adsorb to the hydrophobic alkyl chain of the linker. Only the nitrogen atoms of the amine groups are preferential sorption sites for water molecules via hydrogen bonds, which results in a smaller sensitivity. Because of the similar structure of the dodecylamine ligands and DA linker molecules, it is conceivable that the unexchanged ligands with their relatively long alkyl chains (-C₁₂H₂₅) are involved in the sensing mechanism as well. Consequently, the sensor responses of DA AuC₆ and AuC₈ are not very different for the various analytes and presumably depend primarily on the diffusion behavior and polarity of the analytes as well as on the pore size of the composite.

Finally, the BDTC sensors exhibit highest sensitivities to the hydrophilic analytes 1-propanol (3.6% for AuC₆; 4.6% for AuC₈) and water (2.5% for AuC₆; 2.1% for AuC₈). Because of the low density of BDTC composites compared to DT and DA sensors, which corresponds to a high film porosity, the pore filling process is significantly involved in the sensing mechanism. In addition, swelling of the BDTC composites will occur. Both the significant porosity and swelling induce a high sensitivity especially to hydrophilic analytes compared to the DA sensors. Because of the branched non-linear bound functional groups, with each group consisting of two sulfur atoms, the BDTC molecules preferentially provide hydrophilic sorption sites for the detection of 1-propanol and water (see **Figure 9**).



Furthermore, the BDTC sensors show a significant sensitivity to nonpolar analytes such as toluene and 4-methyl-2-pentanone due to the hydrophobicity of the alkyl chains. Because of the high

selectivity to 1-propanol and water, the BDTC composites are well-suited candidates for the detection of hydrophilic vapor compounds. Compared to the DT films, the sensitivities of DA

TABLE 3 | Selection of research works reporting on chemiresistive NP composites used for VOC sensing comparing the sensitivity (at a vapor concentration of 1,000 ppm), the limit of detection (LOD), the selectivity, the response time (t_{90}) and the long-time stability of different organic linker molecules to toluene (non-polar) and water (polar) vapor as volatile compounds. In particular, the following linker molecules are considered: polymers, i.e. DT-alkyl dithiols, DA-alkyl diamines, BDTC-alkyl bisdithiocarbamates, TT-alkyl trithiols, TOABr-tetraoctylammonium bromide; disulfide-functionalized dendrimers, i.e. PPh-poly phenylenes, PPI-poly propylene imines, PAA-poly (amidoamines); thiol-functionalized DNA oligomers, i.e. Poly A-adenines, Poly C-cytosines, Poly T-thymines. *not available, ++ very high, + high, - low, - very low.

Sensor Parameter	This Work AuNP/Polymers			Schlicke et al. (2021) AuNP/Polymers	Garg et al. (2010) AuNP/Polymers	Ibañez and Zamborini, (2008) AuNP/Polymers	Krasteva et al. (2002), Vossmeier et al. (2002) AuNP/Dendrimers			Fu et al. (2013) AuNP/DNA Oligomers	
	DT	DA	BDTC	DT	TT	TOABr	PPh	PPI	PAA	Poly A	Poly B
Linker molecule	DT	DA	BDTC	DT	TT	TOABr	PPh	PPI	PAA	Poly A	Poly B
	AuC8			AuC6						Poly A	Poly T
Sensitivity at 1,000 ppm (%):											
Toluene:	1.9	0.6	0.6	~2.1	10	17.7	~7.0	~0.6	~1.4	0.19-0.82	
Water:	~0.1	~0.4	0.6	~0.2	n.a.*	n.a	~0.1	~0.3	0.0	n.a	
Detection limit LOD (ppm):											
Toluene:	10	25	8	n.a	n.a	<13	<5	n.a.	n.a.	221	
Water:	200	25	10	n.a	n.a	n.a	n.a.	n.a.	n.a.	n.a.	
Selectivity:											
Toluene:	++	-	-	++	++	-	++	-	no	+	
Water:	-	+	++	-	n.a	n.a (+)	-	-	++	n.a	
Response time t_{90} (s):	at 2000 ppm			at 8000 ppm		at 1000 ppm		at 100 ppm			
Toluene:	2	7	20	~40	~5	~5	~25	n.a.	n.a.	n.a.	
Water:	5	9	7	~20	n.a.	n.a.	n.a.	n.a.	~50	n.a.	
Long-time stability (% drop in response):					<10 during 6 months	<20 during 16 months					
Toluene	-	-	+	n.a.			n.a.			n.a.	

and BDTC composites do not correlate clearly with the alkyl chain length to all analytes. For the BDTC composites, this needs more investigation in detail with stronger variation in the alkyl length. All sensitivities and selectivities are compared with results from the literature in **Table 3**.

3.3.2 Response and Recovery Times

The response and recovery times of the AuNP composite sensors vary with analyte, analyte concentration as well as of the class of interlinking molecules while the differences in the chain length only play a minor role (for details see **Supplementary Information**) indicating a similar structure within a class of linkers. The DT sensors have extremely short response and recovery times of approximately 2 s, the DA composites respond within approximately 5 s and need ~7 s to recover. The highest response and recovery times were measured for the BDTC sensors with approximately 6–20 s and more than 30 s, respectively probably due to the considerable higher thickness of the sensing composite. Interestingly, the BDTC sensors provide especially short response times for the detection of water (see **Figure 9**) presumably due to the small size and the increased adsorption dynamics of the water molecules. In summary, these data indicate that the DT and DA sensors particularly exhibit high reversibility.

3.3.3 Further Sensor Properties

The relative change in the electrical resistance to toluene, 4-methyl-2-pentanone, water, and 1-propanol as a function of

analyte concentration is shown in **Figures 10, 11**. Due to the high signal to noise ratio, the detection of analyte concentrations down to 100 ppm or below is possible for all used test vapors. All composite films reveal non-linear isothermal curves for the different analytes with different concentrations measured at room temperature. The higher the analyte concentration, the

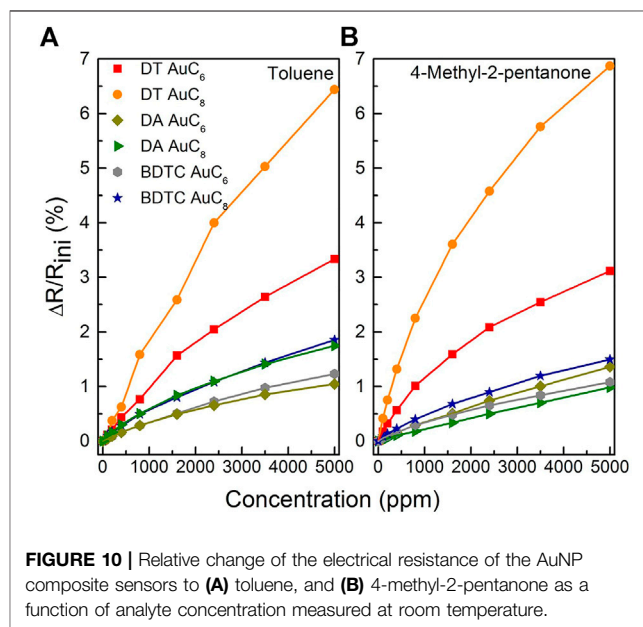
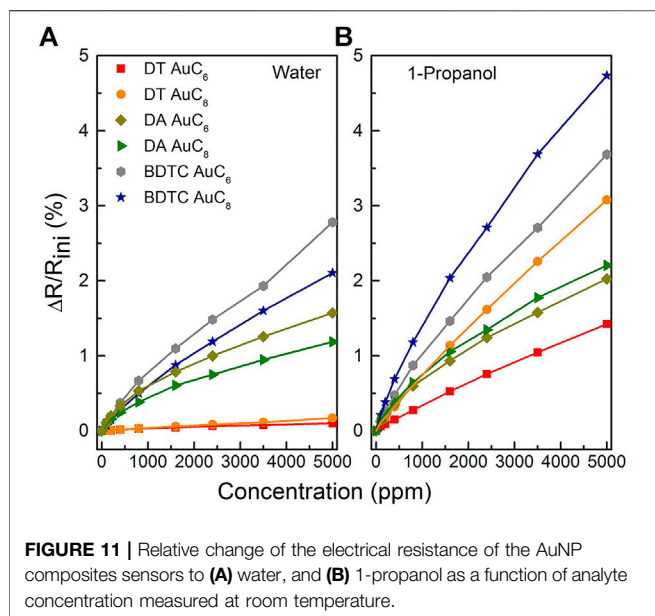


FIGURE 10 | Relative change of the electrical resistance of the AuNP composite sensors to (A) toluene, and (B) 4-methyl-2-pentanone as a function of analyte concentration measured at room temperature.



smaller is the increase in sensitivity until saturation is achieved. Summarizing, the DT composite responses display particularly selectivity towards toluene and 4-methyl-2-pentanone depending on the chain length of the linker molecules. The DA sensors are characterized by only a slight change in sensitivity when dosing them with different solvent vapors, which leads to a non-selective sensor response. In contrast, the BDTC composites reveal a high selectivity to hydrophilic analytes.

Table 3 shows a selection of research works reporting on chemiresistive AuNP composites used for VOC sensing in comparison with the composites prepared within this study. The sensitivities of AuNP composites to toluene and water perfectly match with those reported in the literature (Schlicke et al., 2021). Also in agreement with the literature, our dithiol based sensor is highly selective to non-polar compounds such as toluene in contrast to polar vapors such as water. All our composite sensors show remarkably short response times with $t_{90} \leq 20$ s, whereas competing sensors need longer time to show an equivalent response even when the concentration of vapor doses is higher (Schlicke et al., 2021). The limits of detection (LOD) of the prepared sensors amounts to ~ 8 –200 ppm dependent on the material and analyte and are comparable to the sensors known in the literature. As found in the literature, AuNP/polymer sensors consisting of alkyl trithiols (TT) and tetraoctylammonium bromide (TOABr) are also suitable candidates for VOC sensing. According to **Table 3**, TT and TOABr composite films clearly reveal higher sensitivities to toluene (by one order of magnitude) compared to our DT, DA and BDTC composites, which is attributed to the differing chemical structure of the linker molecules (Ibañez and Zamborini, 2008; Garg et al., 2010) and a dissimilar sensing mechanism (Ibañez and Zamborini, 2008). Whereas, TT composites are very selective to toluene similar to our DT sensors, TOABr sensors are nearly non-selective to non-polar VOCs (Ibañez and Zamborini, 2008). Interestingly, both sensor

types reveal also very short response times of ~ 5 s to toluene comparing well with those of our DT and DA composite films. Moreover, with only a resistance drop in the sensor response by less than 10% (TT) and 20% (TOABr) respectively, they are highly long-time stable against degradation under atmospheric conditions. This is presumably due to the absence of thiols (TOABr) or the ability of multidentate binding (TT) both avoiding the proposed aging mechanism by particle destabilization by ozone oxidation of thiols followed by linker loss (Joseph et al., 2009). It is expected that our DA and BDTC sensors exhibit for a similar reason a comparable improved long-time stability against aging compared to our DT sensors. However, this was not subject of this work and will be investigated elsewhere. Finally, AuNP composite sensors based on disulfide-functionalized dendrimers, i.e. poly phenylenes (PPh), poly propylene imines (PPI), and poly amidoamines (PAA) (Krasteva et al., 2002; Vossmeier et al., 2002), or thiol-functionalized DNA oligomers containing adenines (Poly A), cytosines (Poly C), and thymines (Poly T), as linker molecules have proven to be promising for vapor sensing. As can be seen from **Table 3**, dendrimeric AuNP composites show sensitivities to toluene in the range of $\sim 7\%$ (PPh) to $\sim 0.6\%$ (PPI), whereas their sensitivity to polar vapors, i.e. water, is significantly lower. In particular, AuNP/PPh sensors reveal a very small LOD to toluene of 5 ppm or lower and a response time t_{90} of ~ 25 s (Krasteva et al., 2002; Vossmeier et al., 2002). Moreover, their selectivity to toluene and water compares directly with our DT composite films. PPI-based AuNP sensors are less selective to both toluene and water, while PAA-based AuNP sensors are highly selective to water (like the BDTC sensors), but show a slow response with a response time t_{90} of ~ 50 s. In contrast, DNA-based AuNP composites are selective to toluene with sensitivities in the range of 0.19 %–0.82% and exhibit a LOD of 221 ppm (Fu et al., 2013). The latter are not as powerful as AuNP/organic sensors (DT, DA, BDTC, TT, TOABr) and AuNP/dendrimer sensors (PPh, PPI, PAA), but are proposed to enhance the specificity in chemical sensing (Fu et al., 2013).

4 CONCLUSION

In this study, organically interlinked AuNP networks of dithiols, diamines, and bisdithiocarbamates were prepared by using automated layer-by-layer self-assembly. The chemical composition of the NP networks was investigated by XPS. The electrical and vapor-sensing properties as well as the sensor mechanism of the composite films were studied and discussed in detail. In conclusion, the following results were achieved:

- The XPS analysis demonstrates the inclusion of residual solvents in the film material for all composites. The DT composites exhibit a complete ligand-linker exchange. 80% of the linker molecules are doubly bound to the NP surface resulting in a high degree of interlinkage. The XPS analysis reveals an inadequate linker assembly of DA molecules due to the statistical exchange process of homogeneous ligands that leads to a small degree of interlinkage and a high density due to

residual ligands. For the BDTC composites was found that both sulfur species of one functional group of the BDTC molecule are bound to the AuNPs. The sensor films contain residual ligands, which indicates an incomplete ligand-linker exchange. But 60% of the BDTC molecules are bound to the NP surface on both ends which corresponds to a high degree of interlinkage.

- b) All films show ohmic current-voltage characteristics and electrical conductivities in the range of 10^{-2} – 10^{-4} Ω^{-1} cm^{-1} at room temperature. DT and DA sensors offer very dense films whereas highly porous BDTC films are formed due to the branched molecule structure.
- c) The DT composites exhibit the highest sensitivities followed by DA and BDTC sensors. The DT sensors show high selectivity towards the hydrophobic test vapors toluene and 4-methyl-2-pentanone. The DA and BDTC sensors reveal high selectivities to the hydrophilic analytes 1-propanol and water. Induced swelling of the film material is the dominating sensor mechanism for all studied linker types. The overall sensor response demonstrates a mixture of the amount of sorbed analyte, the swellability, and filling the pores of the AuNP composites. The obtained results demonstrate that DT composites are ideal candidates for chemical sensor applications due to their excellent sensing properties. DA sensors are not very promising candidates because of the hardly controllable and incomplete ligand-linker exchange. There is high potential for BDTC sensors as novel chemiresistive materials because of the appreciable sensing properties that make further research on molecule integration and sensor evaluation useful. Additionally, the BDTC sensors may exhibit improved stability against aging caused by oxidation in atmosphere since the BDTC composite films are not composed of thiols (Joseph et al., 2009). However, further investigations are necessary to confirm that.

REFERENCES

- Andres, R. P., Bielefeld, J. D., Henderson, J. I., Janes, D. B., Kolagunta, V. R., Kubiak, C. P., et al. (1996). Self-Assembly of a Two-Dimensional Superlattice of Molecularly Linked Metal Clusters. *Science* 273 (5282), 1690–1693. doi:10.1126/science.273.5282.1690
- Broza, Y. Y., Vishinkin, R., Barash, O., Nakhleh, M. K., and Haick, H. (2018). Synergy between Nanomaterials and Volatile Organic Compounds for Non-invasive Medical Evaluation. *Chem. Soc. Rev.* 47 (13), 4781–4859. doi:10.1039/c8cs00317c
- Daskal, Y., Tauchnitz, T., Güth, F., Dittrich, R., and Joseph, Y. (2017). Assembly Behavior of Organically Interlinked Gold Nanoparticle Composite Films: A Quartz Crystal Microbalance Investigation. *Langmuir* 33 (43), 11869–11877. doi:10.1021/acs.langmuir.7b01974
- Ehsani, M., Rahimi, P., and Joseph, Y. (2021). Structure-Function Relationships of Nanocarbon/Polymer Composites for Chemiresistive Sensing: A Review. *Sensors* 21 (9), 3291. Available at: URL:https://www.mdpi.com/1102860. doi:10.3390/s21093291
- Evans, S. D., Johnson, S. R., Cheng, Y. L., and Tiehan, S. (1999). Vapour Sensing Using Hybrid Organic–Inorganic Nanostructured Materials. *J. Mater. Chem.* 10 (1), 183–188. Available at: URL: https://pubs.rsc.org/en/content/articlehtml/2000/jm/a903951a. doi:10.1039/a903951a
- Franke, M. E., Koplin, T. J., and Simon, U. (2006). Metal and Metal Oxide Nanoparticles in Chemiresistors: Does the Nanoscale Matter? *Small* 2 (1), 36–50. doi:10.1002/sml.200500261

DATA AVAILABILITY STATEMENT

The raw data supporting the conclusion of this article will be made available by the authors, without undue reservation.

AUTHOR CONTRIBUTIONS

Conceptualization, TT, YJ; Formal analysis, TT, YD, and YJ; Methodology, YD, MG, RD; Project administration, YJ; Resources, FM, YJ; Writing—original draft, TT; Writing—review and editing, YD, RD, MG, FM, and YJ. All authors have read and agreed to the published version of the manuscript.

FUNDING

Open Access Funding by the Publication Fund of the TU Bergakademie Freiberg.

ACKNOWLEDGMENTS

The author thanks J. Adam, M. Haverkamp, and A. Reichel for their support during sample preparation and experiments.

SUPPLEMENTARY MATERIAL

The Supplementary Material for this article can be found online at: <https://www.frontiersin.org/articles/10.3389/fsens.2022.907443/full#supplementary-material>

- Fu, K., Li, S., Jiang, X., Wang, Y., and Willis, B. G. (2013). DNA Gold Nanoparticle Nanocomposite Films for Chemiresistive Vapor Sensing. *Langmuir* 29 (46), 14335–14343. doi:10.1021/la402626p
- Garg, N., Mohanty, A., Lazarus, N., Schultz, L., Rozzi, T. R., Santhanam, S., et al. (2010). Robust Gold Nanoparticles Stabilized by Trithiol for Application in Chemiresistive Sensors. *Nanotechnology* 21 (40), 405501. Available at: URL: https://iopscience.iop.org/article/10.1088/0957-4484/21/40/405501. doi:10.1088/0957-4484/21/40/405501
- Grate, J. W., Nelson, D. A., and Skaggs, R. (2003). Sorptive Behavior of Monolayer-Protected Gold Nanoparticle Films: Implications for Chemical Vapor Sensing. *Anal. Chem.* 75 (8), 1868–1879. doi:10.1021/ac0206364
- Haick, H. (2007). Chemical Sensors Based on Molecularly Modified Metallic Nanoparticles. *J. Phys. D: Appl. Phys.* 40 (23), 7173–7186. doi:10.1088/0022-3727/40/23/s01. Available at: URL: https://iopscience.iop.org/article/10.1088/0022-3727/40/23/S01.
- Han, L., Daniel, D. R., Maye, M. M., and Zhong, C.-J. (2001). Core–Shell Nanostructured Nanoparticle Films as Chemically Sensitive Interfaces. *Anal. Chem.* 73 (18), 4441–4449. doi:10.1021/ac0104025
- Hartwig, M., Zichner, R., and Joseph, Y. (2018). Inkjet-Printed Wireless Chemiresistive Sensors—A Review. *Chemosensors* 6 (4), 66. doi:10.3390/chemosensors6040066
- Ibañez, F. J., and Zamborini, F. P. (2008). Chemiresistive Sensing of Volatile Organic Compounds with Films of Surfactant-Stabilized Gold and Gold–Silver Alloy Nanoparticles. *ACS Nano* 2 (8), 1543–1552. doi:10.1021/nn800109q
- Jiang, G., Wang, L., and Chen, W. (2007). Studies on the Preparation and Characterization of Gold Nanoparticles Protected by Dendrons. *Mater. Lett.* 61 (1), 278–283. doi:10.1016/j.matlet.2006.04.110

- Joseph, Y., Besnard, I., Rosenberger, M., Guse, B., Nothofer, H.-G., Wessels, J. M., et al. (2003). Self-Assembled Gold Nanoparticle/Alkanedithiol Films: Preparation, Electron Microscopy, XPS-Analysis, Charge Transport, and Vapor-Sensing Properties. *J. Phys. Chem. B* 107 (30), 7406–7413. doi:10.1021/jp030439o
- Joseph, Y. (2004). Chemiresistor Coatings from Pt- and Au-Nanoparticle/nonanedithiol Films: Sensitivity to Gases and Solvent Vapors. *Sensors Actuators B Chem.* 98 (2-3), 188–195. Available at: URL. doi:10.1016/j.snb.2003.10.006
- Joseph, Y., Guse, B., and Nelles, G. (2009). Aging of 1,ω-Alkyldithiol Interlinked Au Nanoparticle Networks. *Chem. Mat.* 21 (8), 1670–1676. doi:10.1021/cm803407n
- Joseph, Y., Guse, B., Vossmeier, T., and Yasuda, A. (2008). Gold Nanoparticle/Organic Networks as Chemiresistor Coatings: The Effect of Film Morphology on Vapor Sensitivity. *J. Phys. Chem. C* 112 (32), 12507–12514. doi:10.1021/jp8013546
- Joseph, Y., Krasteva, N., Besnard, I., Guse, B., Rosenberger, M., Wild, U., et al. (2004). Gold-nanoparticle/organic Linker Films: Self-Assembly, Electronic and Structural Characterisation, Composition and Vapour Sensitivity. *Faraday Discuss.* 125 (0), 77–97. doi:10.1039/b302678g; discussion 99–116. Available at: URL: <https://pubs.rsc.org/en/content/articlehtml/2004/fd/b302678g>.
- Joseph, Y., Peić, A., Chen, X., Michl, J., Vossmeier, T., and Yasuda, A. (2007). Vapor Sensitivity of Networked Gold Nanoparticle Chemiresistors: Importance of Flexibility and Resistivity of the Interlinkage. *J. Phys. Chem. C* 111 (34), 12855–12859. doi:10.1021/jp072053+
- Ketelsen, B., Yesilmen, M., Schlicke, H., Noei, H., Su, C.-H., Liao, Y.-C., et al. (2018). Fabrication of Strain Gauges via Contact Printing: A Simple Route to Healthcare Sensors Based on Cross-Linked Gold Nanoparticles. *ACS Appl. Mat. Interfaces* 10 (43), 37374–37385. doi:10.1021/acsami.8b12057
- Krasteva, N., Guse, B., Besnard, I., Yasuda, A., and Vossmeier, T. (2003). Gold nanoparticle/PPI-Dendrimer Based Chemiresistors. *Sensors Actuators B Chem.* 92 (1-2), 137–143. doi:10.1016/s0925-4005(03)00250-8
- Krasteva, N., Besnard, I., Guse, B., Bauer, R. E., Müllen, K., Yasuda, A., et al. (2002). Self-Assembled Gold Nanoparticle/Dendrimer Composite Films for Vapor Sensing Applications. *Nano Lett.* 2 (5), 551–555. doi:10.1021/nl020242s
- Leff, D. V., Brandt, L., and Heath, J. R. (1996). Synthesis and Characterization of Hydrophobic, Organically-Soluble Gold Nanocrystals Functionalized with Primary Amines. *Langmuir* 12 (20), 4723–4730. doi:10.1021/la960445u
- Maiti, S., Maiti, S., Joseph, Y., Wolf, A., Brütting, W., Dorfs, D., et al. (2018). Electronically Coupled, Two-Dimensional Assembly of Cu_{1.1}S Nanodiscs for Selective Vapor Sensing Applications. *J. Phys. Chem. C* 122 (41), 23720–23727. doi:10.1021/acs.jpcc.8b05276
- Morf, P., Raimondi, F., Nothofer, H.-G., Schnyder, B., Yasuda, A., Wessels, J. M., et al. (2006). Dithiocarbamates: Functional and Versatile Linkers for the Formation of Self-Assembled Monolayers. *Langmuir* 22 (2), 658–663. doi:10.1021/la052952u
- Potyrailo, R. A. (2017). Toward High Value Sensing: Monolayer-Protected Metal Nanoparticles in Multivariable Gas and Vapor Sensors. *Chem. Soc. Rev.* 46 (17), 5311–5346. doi:10.1039/c7cs00007c
- Reichhelm, A., Haubold, D., and Eychmüller, A. (2017). Ligand Versatility in Supercrystal Formation. *Adv. Funct. Mat.* 27 (39), 1700361. doi:10.1002/adfm.201700361
- Samadi Khoshkhoo, M., Joseph, Y., Maiti, S., Schreiber, F., Chassé, T., and Scheele, M. (2018). Tunable Charge Transport in Hybrid Superlattices of Indium Tin Oxide Nanocrystals and Metal Phthalocyanines-Toward Sensing Applications. *Adv. Mat. Interfaces* 5 (9), 1701623. doi:10.1002/admi.201701623
- Samadi Khoshkhoo, M., Lox, J. F. L., Koitzsch, A., Lesny, H., Joseph, Y., Lesnyak, V., et al. (2019). Highly Conductive Copper Selenide Nanocrystal Thin Films for Advanced Electronics. *ACS Appl. Electron. Mat.* 1 (8), 1560–1569. doi:10.1021/acsaelm.9b00323
- Schlicke, H., Behrens, M., Schröter, C. J., Dahl, G. T., Hartmann, H., and Vossmeier, T. (2017). Cross-Linked Gold-Nanoparticle Membrane Resonators as Microelectromechanical Vapor Sensors. *ACS Sens.* 2 (4), 540–546. doi:10.1021/acssensors.6b00831
- Schlicke, H., Bittinger, S. C., Noei, H., and Vossmeier, T. (2021). Gold Nanoparticle-Based Chemiresistors: Recognition of Volatile Organic Compounds Using Tunable Response Kinetics. *ACS Appl. Nano Mat.* 4 (10), 10399–10408. doi:10.1021/acsnm.1c01892
- Schlicke, H., Bittinger, S. C., and Vossmeier, T. (2020). Lithographic Patterning and Selective Functionalization of Metal Nanoparticle Composite Films. *ACS Appl. Electron. Mat.* 2 (11), 3741–3748. doi:10.1021/acsaelm.0c00770
- Shipway, A. N., Katz, E., and Willner, I. (2000). Nanoparticle Arrays on Surfaces for Electronic, Optical, and Sensor Applications. *ChemPhysChem* 1 (1), 18–52. doi:10.1002/1439-7641(20000804)1:1<18::aid-cphc18>3.0.co;2-l
- Song, L., Huang, Y., Nie, Z., and Chen, T. (2020). Macroscopic Two-Dimensional Monolayer Films of Gold Nanoparticles: Fabrication Strategies, Surface Engineering and Functional Applications. *Nanoscale* 12 (14), 7433–7460. doi:10.1039/c9nr09420b
- Squillaci, M. A., Stoeckel, M.-A., and Samori, P. (2019). 3D Hybrid Networks of Gold Nanoparticles: Mechanoresponsive Electrical Humidity Sensors with On-Demand Performances. *Nanoscale* 11 (41), 19319–19326. doi:10.1039/c9nr05336k
- Toda, M., Joseph, Y., and Berger, R. (2010). Swelling of Composite Films at Interfaces. *J. Phys. Chem. C* 114 (5), 2012–2017. doi:10.1021/jp9087578
- Vossmeier, T., Guse, B., Besnard, I., Bauer, R. E., Müllen, K., and Yasuda, A. (2002). Gold Nanoparticle/Polyphenylene Dendrimer Composite Films: Preparation and Vapor-Sensing Properties. *Adv. Mater.* 14 (3), 238–242. doi:10.1002/1521-4095(20020205)14:3<238::aid-adma238>3.0.co;2-#
- Wang, L., Shi, X., Kariuki, N. N., Schadt, M., Wang, G. R., Rendeng, Q., et al. (2007). Array of Molecularly Mediated Thin Film Assemblies of Nanoparticles: Correlation of Vapor Sensing with Interparticle Spatial Properties. *J. Am. Chem. Soc.* 129 (7), 2161–2170. doi:10.1021/ja0673074
- Wuelfing, W. P., Green, S. J., Pietron, J. J., Cliffl, D. E., and Murray, R. W. (2000). Electronic Conductivity of Solid-State, Mixed-Valent, Monolayer-Protected Au Clusters. *J. Am. Chem. Soc.* 122 (46), 11465–11472. doi:10.1021/ja002367+
- Xue, Y., Li, X., Li, H., and Zhang, W. (2014). Quantifying Thiol-Gold Interactions towards the Efficient Strength Control. *Nat. Commun.* 5 (1), 4348–4349. doi:10.1038/ncomms5348 Available at: URL: <https://www.nature.com/articles/ncomms5348?origin=ppub>.
- Yang, M., Yang, Y., Liu, Y., Shen, G., and Yu, R. (2006). Platinum Nanoparticles-Doped Sol-Gel/Carbon Nanotubes Composite Electrochemical Sensors and Biosensors. *Biosens. Bioelectron.* 21 (7), 1125–1131. Available at: URL: doi:10.1016/j.bios.2005.04.009
- Yonezawa, T., Yasui, K., and Kimizuka, N. (2001). Controlled Formation of Smaller Gold Nanoparticles by the Use of Four-Chained Disulfide Stabilizer. *Langmuir* 17 (2), 271–273. doi:10.1021/la001247c
- Zhang, H.-L., Evans, S. D., Henderson, J. R., Miles, R. E., and Shen, T.-H. (2002). Vapour Sensing Using Surface Functionalized Gold Nanoparticles. *Nanotechnology* 13 (3), 439–444. doi:10.1088/0957-4484/13/3/339 Available at: URL: <https://iopscience.iop.org/article/10.1088/0957-4484/13/3/339/meta>.

Conflict of Interest: The authors declare that the research was conducted in the absence of any commercial or financial relationships that could be construed as a potential conflict of interest.

Publisher's Note: All claims expressed in this article are solely those of the authors and do not necessarily represent those of their affiliated organizations, or those of the publisher, the editors and the reviewers. Any product that may be evaluated in this article, or claim that may be made by its manufacturer, is not guaranteed or endorsed by the publisher.

Copyright © 2022 Tauchnitz, Daskal, Dittrich, Günthel, Mertens and Joseph. This is an open-access article distributed under the terms of the Creative Commons Attribution License (CC BY). The use, distribution or reproduction in other forums is permitted, provided the original author(s) and the copyright owner(s) are credited and that the original publication in this journal is cited, in accordance with accepted academic practice. No use, distribution or reproduction is permitted which does not comply with these terms.